

THE SINGULARITY OF EARDLEY, SMARR, AND CHRISTODOULOU

Charles Hellaby
Dept. of Applied Maths
University of Cape Town
Rondebosch 7700
South Africa

and

Kayll Lake
Dept of Physics
Queen's University
Kingston
Ontario
K7L 3N6
Canada

Abstract

A strange kind of singularity in some Tolman models was found by Eardley and Smarr (1978) in a numerical study, and more recently by Christodoulou (1984) in a mathematical proof of a violation of cosmic censorship in a particular class of models. In a collapsing dust cloud, if the crunch singularity occurs first at the origin, then, given some apparently reasonable conditions, it can be shown that this single point on the crunch surface emits light rays, and is therefore naked, at least locally and sometimes globally. This “ESC” singularity is a single point in standard coordinates, and appears at the centre of symmetry on the crunch surface, yet it emits an infinite set of light rays. If the dust cloud of the Tolman model is joined to a Schwarzschild exterior, then some of those rays can reach future null infinity, and it can be seen for a finite length of time.

The conditions under which this singularity occurs are generalised, and approximate forms for the rays emerging from it are derived. The paths of the light rays in the vicinity of this singularity are integrated numerically for a particular case, and a causal diagram is also calculated numerically for this same case. The conditions for existence agree with those of Eardley and Smarr, but the causal diagram is different in one respect. The calculation of the orientation of the crunch surface at the ESC singularity is done for the general case, and it is found to be heavily dependent on the path chosen to approach that point. Lastly, a reasonable continuity condition is put forward which is not satisfied by models containing an ESC singularity. The condition is that the derivative of the density with respect to the mass at constant time must be zero at the origin.

1 Introduction

In 1984, a very interesting violation of cosmic censorship was published by Christodoulou (1984). In outline, he took a spherically symmetric dust cloud of finite size, and allowed it to collapse. The exterior was described by the Schwarzschild vacuum, while the interior consisted of an elliptic Tolman model, whose arbitrary functions were chosen such that the cloud was initially at rest, and the density fell to zero at the surface of the cloud. Further, he imposed a strong continuity condition at the origin, which is important for the proof, but seems entirely reasonable. Specifically, the condition was that the density must be an even, C^∞ function of r , even when r is carried through zero to negative values. Obviously the intent was to ensure that there is nothing irregular about the origin in the initial conditions. In this model, the crunch singularity occurs first at the centre of symmetry, $r = 0$, and spreads to increasing radius with time, thus ensuring that the model is free of shell crossings (Hellaby and Lake 1985). The crunch singularity joins to the future singularity of the exterior Schwarzschild manifold, and the apparent horizon joins to the Schwarzschild event horizon. Christodoulou then showed that, for a certain class of models, the first ray to emerge from that initial point on the singularity, could reach the exterior of the cloud a finite time before the cloud entered the horizon, and escape to infinity, thus constituting a global violation of cosmic censorship. (A ray is said to emerge from a singularity if its path can be traced back to arbitrarily small affine distances from that singularity.)

This singularity was first discovered in a study of numerical relativity conducted by Eardley and Smarr (1978). The primary aim of their paper was to investigate ways of slicing the spacetime to obtain the best coverage by the numerical grid, whilst avoiding the singularity. Their model was also a dust cloud surrounded by vacuum, but the interior was a parabolic Tolman metric, and they calculated a large variety of cases to compare their results with the known analytic solutions. They too found that, in models where this singularity existed, light could be propagated from the initial

singular point, and could in some cases reach future null infinity. The three conformal diagrams they drew for these spacetimes (q.v.) show respectively no violation of cosmic censorship, a local violation, and a global violation.

In their paper they comment that this singularity “has hitherto escaped notice in these models for 40 years”, and they find it “surprising that these phenomena occur in the family of Tolman-Bondi spacetimes, which are thought to be well understood”. Perhaps one reason is that Eardley and Smarr give no explanation of this singularity, other than tabulating which types of model it occurs in, nor do they say how they came across it, or derived the conditions for its existence. In the analytical treatment, the existence of rays emerging from this singularity does not become apparent without carefully examining the geodesic equation. Since no general solution is known, even for the radial null geodesics, this requires a purpose-built method.

And indeed the existence of this singularity *is* surprising, especially since the crunch surface can be shown to be entirely spacelike everywhere else. However, careful examination of the arguments shows that this result is not always valid for points that are both close to the origin and near the crunch.

More recently Newman (1986) studied the strength of this singularity, using a model similar to Christodoulou’s. He found that it obeyed his “limiting focussing condition”, but not his “strong limiting focussing condition”. He also drew a causal diagram similar to one of Eardley and Smarr’s, but time symmetric. Ori and Piran (1987) have shown that this type of singularity also exists in self-similar collapse models with a soft equation of state, while Lake (1988) and Waugh and Lake (1988) have shown that all self-similar models, with or without pressure, generate strong curvature singularities at these singular points.

I have chosen to call this central point on the crunch surface, together with its effects, the ESC singularity, after its discoverers, though Eardley and Smarr named it a shell focussing singularity. I have not used that name, as the shells of matter are “focussed” into the crunch singularity whether or not there is an ESC singularity. One might alternatively call it a light focussing singularity — a name which would also apply to certain singularities found in the Vaidya metric which seem to have similar causal diagrams (Hiscock et al 1982, Kuroda 1984, Papapetrou 1985, Waugh & Lake 1986).

There is no accepted definition of a singularity in General Relativity (Tipler, Clarke, and Ellis 1979) but, loosely speaking, a singularity is a point or locus of points where the Einstein equations break down, and which is often associated with divergences in quantities like the density and the Kretschmann scalar. Therefore, since nothing can be said about singular points themselves, the study of a singularity is actually the study of the limiting behaviour as the singular point is approached.

The limiting behaviour of the ESC singularity is investigated in this paper, with the aim of tracing the paths of the rays that emerge from it, and in particular, a causal diagram is calculated. The emphasis is on the behaviour of the Tolman metric near the ESC singularity, and the question of whether the violation of cosmic censorship is local or global in a Schwarzschild exterior is not of great concern here. The spacelike, null, or timelike character of the singularity is also investigated. Only some of the cases of interest have been covered, and conflicting results have emerged, so the conclusions can only be tentative.

2 The Model

The Tolman metric (Lemaître 1933, Tolman 1934, Datt 1938, Bondi 1947) represents a distribution of pressure free matter (dust) that is spherically symmetric, but inhomogeneous in the radial direction.

It is written in synchronous, comoving coordinates, so that $g_{tt} = -1$, and $g_{ti} = 0$ ($i = 1, 2, 3$), and the tangent vector of the particles of matter is $u^\alpha = (1, 0, 0, 0)$. The cosmological constant, Λ , will be neglected and geometric units such that $G = 1$ and $c = 1$ will be used throughout. Thus the metric is,

$$ds^2 = -dt^2 + \frac{R'^2(r, t)}{1 + f(r)} dr^2 + R^2(r, t) d\Omega^2, \quad (2.1)$$

where $d\Omega^2 = d\theta^2 + \sin^2 \theta d\phi^2$, $' = \partial/\partial r$, and $\dot{} = \partial/\partial t$ will be used below. The evolution of the areal radius, $R(r, t)$, is found from the Einstein equations, which give

$$\dot{R}^2 = \frac{F(r)}{R} + f(r), \quad (2.2)$$

and has the following parametric solutions;
hyperbolic, $f > 0$,

$$R = \frac{F}{2f}(\cosh \eta - 1), \quad (\sinh \eta - \eta) = \frac{2f^{3/2}(a(r) - t)}{F}; \quad (2.3)$$

parabolic, $f = 0$,

$$R = \left[\frac{9F(a(r) - t)^2}{4} \right]^{1/3}; \quad (2.4)$$

elliptic, $f < 0$,

$$R = \frac{F}{2(-f)}(1 - \cos \eta), \quad (\eta - \sin \eta) = \frac{2(-f)^{3/2}(a(r) - t)}{F}. \quad (2.5)$$

The time reversed parabolic and hyperbolic cases, obtained by writing $(t - a)$ instead of $(a - t)$, are also valid solutions. Unlike the Robertson-Walker models, the big crunch does not necessarily occur simultaneously everywhere, neither are the times of the big bang or maximum expansion simultaneous in general. The hyperbolic and elliptic cases can easily be shown to reduce to the parabolic form for $\eta \rightarrow 0$, i.e. as $t \rightarrow a$, so that all three cases have the same behaviour close to the bang or crunch.

The density is given by

$$8\pi\rho = \frac{F'}{R^2 R'}, \quad (2.6)$$

and the Kretschmann scalar is (e.g. Bondi 1947)

$$K = R^{\alpha\beta\gamma\delta} R_{\alpha\beta\gamma\delta} = \frac{12F^2}{R^6} - \frac{8FF'}{R^5 R'} + \frac{3F'^2}{R^4 R'^2}, \quad (2.7)$$

where $R^{\alpha\beta\gamma\delta}$ is the Riemann tensor.

The functions, F , f , and a , are all arbitrary functions of the coordinate radius r , which allow a coordinate choice, plus the specification of two physically independent quantities. The local time at which $R = 0$ is $a(r)$, and, in the above solutions it is the time of the big crunch. The function $F(r)$ is twice the effective gravitational mass, M , within coordinate radius r (see Bondi 1947). The third function, $f(r)$, determines both the type of time evolution, and the local geometry.

An origin occurs at $r = 0$ if $R(0, t) = 0$ (i.e. $g_{\theta\theta} = g_{\phi\phi} = 0$) for all t . Normally at the origin, F and f both go to zero (though this does not necessarily mean that the time evolution is parabolic). The origin will be regular provided these functions obey

$$f \sim f_0 F^{2/3} \quad (2.8)$$

near $r = 0$. (A more detailed discussion of the evolution at the origin can be found in Hellaby (1985).)

There are two hypersurfaces where the density and the Kretschmann scalar, given by eqs (2.6) and (2.7), diverge; the loci of $R = 0$, and of $R' = 0$. The bang and the crunch are characterised by $R = 0$, while $R' = 0$ represents a shell crossing.

All Tolman models have a big bang singularity, or a big crunch singularity, or both. If the time of the big crunch, $a(r)$, is a decreasing function of r , so that the central shells of matter collapse first, and the outer shells collapse later, then the crunch surface forms a singular origin of growing mass. It is in the centre of this hypersurface, at the moment of its formation that the ESC violation may appear — a singularity within a singularity. (The bang can also display such behaviour in time reverse, but a violation of cosmic censorship does not result.)

The ESC singularity only occurs in certain Tolman models, so it is necessary to place suitable restrictions on the arbitrary functions. Since all the unexpected behaviour happens near the crunch surface, i.e. when η is small, it is sufficient to use a parabolic model, as the other two types have the same behaviour here. It is further assumed that the density is not zero anywhere in the neighbourhood of the origin, so that one may choose the radial coordinate by specifying

$$F = r^3 . \quad (2.9)$$

Thus using (2.4) and (2.9) the evolution of the function R is given by

$$R = \frac{rg^2}{4} , \quad (2.10)$$

where

$$g = [12(a - t)]^{1/3} \quad (2.11)$$

so that

$$\dot{R} = -\frac{2r}{g} , \quad (2.12)$$

and

$$R' = \frac{g^2}{4} + \frac{2ra'}{g} . \quad (2.13)$$

3 The Asymptotic Behaviour of the Rays

From the metric, eq (2.1), the radial null geodesics obey

$$\frac{dt}{dr} = \varepsilon R' = \varepsilon \left(\frac{g^2}{4} + \frac{2ra'}{g} \right) , \quad (3.1)$$

where $\varepsilon = +1$ for outgoing rays, and -1 for incoming rays. This can be converted to an equation in g as the “time” variable using (2.11),

$$g^3 g' = 4ga' - \varepsilon (g^3 + 8a'r) . \quad (3.2)$$

It is now necessary to choose a form for the function $a(r)$. Christodoulou chose it to be a series in even, positive powers of r , in order to fulfil his continuity condition, i.e.

$$a = a_0 + a_1 r^2 + a_2 r^4 + \dots .$$

He found that the violation only occurred if a_1 , the coefficient of r^2 , was non zero. Consequently, the form

$$a = a_0 + a_1 r^m, \quad m > 0, \quad a_1 > 0, \quad (3.3)$$

is chosen so that cases with and without a violation can be studied, as well as other values of m , not considered by him. (If a_1 were less than 0, there would be shell crossings. See Hellaby and Lake 1985) This is also the form assumed by Eardley and Smarr, though they used only integer values of m . (Their r is not quite the same, since they defined r by $M = F/2 = r^3$.) The higher order terms are not important for this investigation, and are omitted here. With this choice, eq (3.2) becomes

$$g^3 g' = 4ma_1 g r^{m-1} - \varepsilon (g^3 + 8ma_1 r^m). \quad (3.4)$$

The constant a_1 may be removed by the transformations

$$s = \frac{r}{a_1^w}, \quad q = \frac{g}{a_1^w}, \quad (3.5)$$

which lead to

$$q^3 q' = 4ma_1^{w(m-3)+1} q s^{m-1} - \varepsilon (q^3 + 8ma_1^{w(m-3)+1} s^m).$$

Here the dash indicates the derivative with respect to s , but since q is always a function of s , and g is always a function of r , no confusion will arise. By setting $w = 1/(3-m)$, the factors of a_1 can be eliminated for all cases except $m = 3$ (the self similar case), viz:

$$q^3 q' = 4mq s^{m-1} - \varepsilon (q^3 + 8ms^m). \quad (3.6)$$

For most cases, then, the paths of the radial light rays do not depend on the value of a_1 , except as a scaling factor.

Firstly the case studied by Christodoulou will be considered, i.e. $m = 2$. Eq (3.6) becomes

$$q^3 q' = 8qs - \varepsilon (q^3 + 16s^2), \quad (3.7)$$

but even in this form there is no obvious solution, nor is it listed by Kamke (1944).

In order to find the behaviour for small s and small q , series expansions will be resorted to. If there is a ray that passes through the origin at $q = 0$, then, for s sufficiently close to zero, it is assumed to follow

$$q = \sum_{i=1}^{\infty} q_i s^{n_i}, \quad (3.8)$$

where $q_i > 0$, $n_i > 0$, and $n_{i+1} > n_i$ for all i . The first term of this series is inserted into eq (3.7),

$$nq_1 s^{4n_1-1} = 8q_1 s^{n_1+1} - \varepsilon (q_1^3 s^{3n_1} + 16s^2), \quad (3.9)$$

and the coefficients of the lowest powers are required to cancel. There are only two values of n which allow this to be done: (i) $n_1 = 2/3$, $q_1 = 12^{1/3}$, and (ii) $n_1 = 1$, $q_1 = 2\varepsilon$. Both of these cases may be extended to higher order. At each stage the solution is found by requiring that $n_i > n_{i-1}$, and that the coefficient equation be consistent with previous results. There is always just one case each time that satisfies these requirements. The results are:

$$(i) \quad q = q_I v^2 - \varepsilon v^3 - \frac{q_I^2}{16} v^4 - \frac{4\varepsilon q_I}{27} v^5 + \dots, \quad (3.10)$$

where $v = s^{1/3}$ and $q_I = 12^{1/3}$;

$$(ii) \quad q = 2\varepsilon s + 3s^2 + \frac{39\varepsilon}{2} s^3 + \frac{387}{2} s^4 + \dots. \quad (3.11)$$

In the second case, s would have to be less than about .1 for the series to converge, but otherwise there is no problem. Also, only the $\varepsilon = +1$ solution of eq (3.11) lies in the positive q region, so the $\varepsilon = -1$ solution for $n = 1$ will be ignored. However, neither of these two solutions has an undetermined constant of integration. One of them, probably (3.10), must be a special case, and would not have a constant, but the other does need one. Using the transformation

$$q = bs$$

to define b as a function of s along the ray, eq (3.7) becomes

$$\frac{db}{ds} = \frac{8}{b^2 s^2} - \frac{1}{s} - \frac{16}{b^3 s^2} - \frac{b}{s}.$$

Since b is finite as $s \rightarrow 0$, this is approximately

$$\frac{db}{ds} = \frac{8(b-2)}{b^3 s^2},$$

which has the solution

$$\frac{1}{3}(b-2)^3 + 3(b-2)^2 + 12(b-2) + 8 \ln(b-2) = -\frac{8}{s} + 8 \ln(C),$$

where C is the constant of integration. As $s \rightarrow 0$, the first term on the right goes to $-\infty$, meaning the last term on the left must dominate the left hand side, so that

$$b = 2 + Ce^{-1/s}, \quad (3.12)$$

and $b \rightarrow 2$, as expected. Since $e^{-1/s}$ goes to zero faster than any power of s , it would not appear in a series expansion. For the same reason, it causes a sharp turn off from the series solution of (3.11) once it does become significant. Of course eq (3.12) is still only an approximation, but it does indicate how the constant of integration appears, and demonstrates that there is a whole family of rays whose limiting form near $s = 0$, $q = 0$ is eq (3.11).

Clearly, eq (3.10) with $\varepsilon = +1$ is the very first ray to escape from the singular origin, and it is the ray that Christodoulou proved to exist. It is effectively the horizon of the ESC singularity, dividing the region that can be causally affected by it from the region that cannot. This ray will be called the "critical ray", all later ones the "post critical rays", and the point from which they emerge the "critical point". The incoming ray which hits this point is the "incoming critical ray" because it has the form (3.10) with $\varepsilon = -1$, rather than the form that all the other incoming rays have (see (3.14) below). If eq (3.10) is put into (2.11), the lowest order term is cancelled, giving

$$t = a_0 + \left[\left(\frac{3}{2} a_1 \right)^2 r^7 \right]^{1/3} \left[1 - \left(\frac{r}{768 a_1} \right)^{1/3} \dots \right], \quad (3.13)$$

and this is the reason for the factor of $x^{7/3}$ in Christodoulou's eq (3.37). (In that equation, $x \propto r$, and $\zeta \propto t - a_0$, while θ is being defined there.)

Before proceeding to the numerical integration, an asymptotic form for the behaviour of the rays near $q = 0$, when $s = s_0 \neq 0$, is needed, and it is found to be

$$s = s_0 - \frac{q^4}{64s_0^2} - \frac{q^5}{160s_0^3} - \frac{q^6}{384s_0^4} - \frac{q^7}{896s_0^5} \left(1 - \frac{s_0}{2} \right) \dots \quad (3.14)$$

Now that the limiting behaviour near $q = 0$ has been found, the ray paths can easily be calculated numerically. Given the form of eq (3.7), it is quite easy to find the higher derivatives of q , so a Taylor series integration is appropriate. The program starts each ray with one of the approximate expressions derived above, but completes the majority of its path numerically, setting the integration interval automatically, based on the relative sizes of the terms in the Taylor expansion. The program first integrates the critical ray outwards till it terminates on the crunch surface, in order to get the scale. Then all other rays are integrated from the crunch surface inwards and backwards in time. The results are shown in fig 1 for s - q coordinates, on 3 different scales. The ray paths in the r - t plane are shown in fig 2, assuming $a_0 = 0$ and $a_1 = 1$. These figures use the convention that incoming rays are plotted on the left side of the origin, with negative s values, and outgoing rays are on the right side with positive s values. The diagram may be thought of as a slice through the origin, showing only the left to right rays, and it makes clear the fact that light rays do in fact pass through the origin. This convention will be maintained for all the ray diagrams. The limitation on the smoothness of these curves is not the program, but the amount of data the graph plotting routine can accept.

Fig 1 & 2 here

It should be remembered that q is not the time, but the cube root of the time before the crunch, and $q = 0$ corresponds to a surface that is curving upwards in the r - t plane. So in fact the rays never go backwards in time, though they may get further away from the crunch surface (in time, or in areal radius) as they go outwards. Given this, the s - q diagram shows the various rays paths much more clearly than the r - t diagram. In all these graphs, the rays are equally spaced in s on the crunch surface. Thus the spacing of the rays at earlier times gives an idea of the expansion between the rays, *in the comoving frame*. It can be seen that rays which pass through the origin and become outgoing well before reaching the crunch surface experience an overall compression, while those which are always incoming and never near the origin have an overall expansion. As the incoming critical ray is approached from either side, the expansion becomes greater, but occurs later in q . In the r - t graphs the expansion seems to occur at very roughly the same time for all rays, and appears to be associated with the "bending over", or decrease in gradient of the rays. On the other hand, rays which are distant from the incoming critical ray are not much affected by the presence of the ESC singularity.

The scaled radius where the outgoing critical ray hits the singularity once again is s_{crit} , and its value in this particular model is .2602, though this value would change if the model were not parabolic, or if there were higher terms in eq (3.3) for the shape of the crunch surface. It is the largest radius which any of the critical rays reach and is therefore the extent of the violation of cosmic censorship within the model, since nothing outside s_{crit} can be causally affected by the ESC singularity. If $M_{crit} = (a_1 s_{crit})^3/2$ is the total mass affected by the violation, and $t_{crit} = a_1^3 s_{crit}^2$ is its duration, then the ratio $M_{crit}/t_{crit} = s_{crit}/2$ is independent of the scale of the model. In order to produce a global violation, it is necessary to put the boundary of the cloud not just within s_{crit} , but before the outgoing critical ray crosses the apparent horizon, where the expansion of the wavefronts of light is zero. The apparent horizon is given by

$$g = 2r , \quad \text{or} \quad q = 2s , \quad (3.15)$$

for the outgoing rays. Along this locus $g' = -1 = q'$. Since the asymptotic form of the post critical rays, eq (3.11), reduces to (3.15) near $s = 0$, it is clear that the rays all fall below this line before turning upwards and crossing it.

4 The Causal Diagram

Having integrated the paths of the light rays, the next step is to calculate a causal diagram in which the light rays are used as coordinates, so that u is constant along the left to right rays, and v is constant along the right to left rays.

Before any calculations can be done, a method of choosing the u and v coordinates must be specified. It is normal to do this by the value of some parameter along a well defined surface. Since the latest post critical rays exist for a vanishingly short time, only surfaces which pass through the critical point parallel to the crunch surface will include them. Therefore the simplest choice is to label each ray by its value of s_0 , where it hits the crunch singularity. Specifically, left to right rays, such as in fig 1, are labelled by

$$u = -s_0 , \tag{4.1}$$

and right to left rays, those in the mirror reflection of fig 1, are labelled by

$$v = s_0 . \tag{4.2}$$

The diagram is calculated numerically in the following manner. Starting with the s - q plane, a grid of lines of constant s is set up, as in fig 3.

Fig 3 here

From the top of each grid line the light ray which hits the singularity there is selected, and labelled by its s_0 value. The ray is integrated backwards from that point, and every time it crosses a grid line the s and q values are recorded. In this way, the s - q plane is covered by a new grid of u and v values. By linear interpolation between these points, it is then possible to calculate a set of u and v values along any given curve (such as $s = \text{const}$ or $t = \text{const}$), which may be plotted in the u - v diagram. Reference to fig 1 shows that, if the incoming critical ray is approached from the left, it has to be labelled with $u = 0$, whereas if it is approached from the right, it appears to be a continuation of the outgoing critical ray, and must be labelled with $u = -s_{crit}$. Thus there is a jump in the value of u across this ray, owing to the later emergence of a whole set of rays between these two limits. There is a similar effect for the v coordinate, and both these jumps must be written into the program. The grid used consists of 55 constant s lines, which is enough to give a reasonably reliable picture.

Fig 4 here

Various families of curves are shown in the u - v diagram in fig 4. The most noticeable feature is the central “lozenge” which the critical point has become, and which is singular, since ρ and K diverge there. The jumps in the u and v values have resulted in two “furrows” which continue out to infinity. In fact the curves are not discontinuous at these jumps but approach them smoothly, confirming that they are a real part of the u - v diagram. Nevertheless, the curves are not null in these furrows. The tangent vectors to the $s = \text{const}$ lines or the $t = \text{const}$ lines are well defined at these points. Thus the furrows are really just stretching the spacetime along two null directions, and the

two sides of each furrow should be identified as the same ray. Another feature is that the $t = \text{const}$ lines tend to avoid the ESC singularity, in other words the rate of change of t with respect to u or v decreases towards the critical point, the lozenge being a single value of t and of r .

The diagrams derived here have one important difference from those drawn by Eardley and Smarr (q.v.), who have omitted the jump in the u and v values. When only half the diagram is drawn, this looks alright, but problems become apparent when it is remembered that the light rays do in fact pass through the origin, and the diagrams must allow a continuation across $r = 0$. Though the presence of these jumps may seem to be unsatisfactory, they are an inevitable feature of the u - v diagram of any spacetime in which a set of rays emerge from a single coordinate point.

What this causal diagram does show most effectively is that the characteristics of the singularity are already beginning to appear just beforehand, since the various curves go continuously through the furrows.

5 The Case of General m

For a better understanding of this singularity, it makes sense to compare the above results with a number of other cases, including those which do not have an ESC singularity.

As noted in the previous section, the case $m = 3$ is qualitatively different from the other cases, since the factor of a_1 cannot be transformed away, so it is not discussed here. (Eardley 1974, and Eardley and Smarr 1979, showed that when $m = 3$ rays only emerge from the critical point if $a_1 \geq a_{1,A} = (52 + 30\sqrt{3})/12$.) For $m \neq 3$, equation (3.6) obtains.

To find those models for which rays may emerge from a central critical point on the crunch surface, eq (3.6) may be solved to lowest order in s , using the first term in eq (3.8), and following the same procedure as above. The results are as follows.

$$\begin{aligned} \text{(a)} \quad m < 3, \quad & \text{(i)} \quad n_1 = m/3, \quad q_1 = 12^{1/3} ; \\ & \text{(ii)} \quad n_1 = 1, \quad q_1 = 2\varepsilon ; \\ \text{(b)} \quad m > 3, \quad & \text{(i)} \quad n_1 = m/3, \quad q_1 = (-8m)^{1/3} ; \\ & \text{(ii)} \quad n_1 = 1, \quad q_1 = -\varepsilon . \end{aligned}$$

Since both s and q must be positive, those rays with $q_1 < 0$ may be ignored. Thus for the $m < 3$ cases, the $n_1 = 1$ solution only exists for $\varepsilon = +1$ (outgoing rays), as in the $m = 2$ case, while for $m > 3$, the $n_1 = 1, \varepsilon = -1$ ray is the only one to exist. Therefore there are no outgoing rays from this point in the $m > 3$ cases, so they do not have ESC singularities. The series may be extended to higher order terms, as before:

$$\text{(a)(i)} \quad q = q_I s^{m/3} - \varepsilon s - \frac{mq_I^2}{4(6+m)} s^{2-m/3} - \frac{2\varepsilon mq_I}{27} s^{3-2m/3} \dots, \quad (5.1)$$

where $q_I = 12^{1/3}$,

$$\text{(a)(ii)} \quad q = 2\varepsilon s + \frac{6}{m} s^{4-m} + \frac{6\varepsilon}{m^2} (17-2m) s^{7-2m} + \frac{12}{m^3} (4m^2 - 66m + 245) s^{10-3m} \dots, \quad (5.2)$$

$$\text{(b)(ii)} \quad q = -\varepsilon s + q_2 s^{m-2} + q_3 s^{2m-5} + q_4 s^{3m-8} \dots, \quad (5.3)$$

where

$$q_2 = \frac{12m}{(m-2)}, \quad q_3 = \frac{384\epsilon m^2}{(m-2)(2m-5)},$$

and

$$q_4 = \frac{192m^3(190m-443)}{(m-2)(2m-5)(3m-8)}.$$

Similarly, an expression is needed for the ray path near $q = 0$ when $s = s_0 \neq 0$. However, since there are non integer powers of s in eq (3.6), it is not suitable for a series expansion of s in powers of q . In this case, the first two terms on the right hand side may be neglected if q is small enough, and integration then leads to

$$q^4 = \frac{32\epsilon m}{(m+1)} (s_0^{m+1} - s^{m+1}), \quad (5.4)$$

and this is sufficient for programming purposes.

The numerical integration of the light ray paths, using the Taylor series method, has been carried out for a selection of m values less than 3. The results of these integrations are plotted in figs 5 and 6 for three m values, and all the graphs have been scaled so that the critical radius, s_{crit} , is at the same point in the diagram. Since the critical ray can be made to reach any desired maximum value of R by adjusting a_1 , this is the best way to compare the behaviour in each case. In fact there are no qualitative differences in behaviour between these four cases, and the only significant quantitative difference is the value of s_{crit} . One can be confident that the conformal diagrams for these cases will differ from fig 4 in equally subtle ways.

Fig 5 & 6 here

For comparison of these cases on the same scale, the outgoing critical rays are plotted on one graph for a variety of m values in fig 7, while the dependence of s_{crit} on m is shown in fig 8. Using the quantities M_{crit} and t_{crit} defined in section 3 above eq (3.15), then $M_{crit}/t_{crit} = (s_{crit})^{3-m}/2$, giving s_{crit} a more direct physical meaning that is independent of a_1 . This ratio is graphed against m in fig 9, and over the range that the data exists, it indicates that the ratio is approaching zero as m goes to 3. Therefore, for an ESC singularity which causes a violation of cosmic censorship of a given duration, the amount of mass affected by the singularity decreases as m approaches 3. On the other hand, for a given affected mass, the duration of the violation increases as m goes to 3. So it is not clear whether the singularity becomes "stronger" or "weaker" towards $m = 3$.

Fig 7, 8, & 9 here

6 Orientation of the Singularity

The big bang and big crunch surfaces in the Tolman metric can easily be shown to be spacelike (almost) everywhere by considering the $\rho = \text{const}$ surfaces. For the hyperbolic case, these surfaces have an (unnormalised) normal vector,

$$n_\alpha \propto \left(\frac{2f^{3/2}}{F}, \left[(\sinh \eta - \eta) \left(\frac{3f'}{2f} - \frac{F'}{F} \right) - \frac{2f^{3/2}a'}{F} \right], 0, 0 \right), \quad (6.1)$$

so that the contraction of n_α is

$$n^\alpha n_\alpha \propto -f + \frac{(1+f) \left[(\sinh \eta - \eta) \left(\frac{3f'}{2f} - \frac{F'}{F} \right) - \frac{2f^{3/2}a'}{F} \right]^2}{(\cosh \eta - 1)^2 \left[\frac{F'}{F}(1 - \phi_+) + \frac{f'}{f} \left(\frac{3}{2}\phi_+ - 1 \right) - \frac{2f^{3/2}a'}{F}\phi_- \right]^2}. \quad (6.2)$$

where

$$\phi_+ = \frac{\sinh \eta (\sinh \eta - \eta)}{(\cosh \eta - 1)^2} \quad (6.3)$$

and

$$\phi_- = \frac{\sinh \eta}{(\cosh \eta - 1)^2}. \quad (6.4)$$

Clearly, this is negative for $\eta \rightarrow 0$, so that the surface is spacelike. A similar argument applies for the elliptic case, taking both $\eta \rightarrow 0$, and $\eta \rightarrow 2\pi$, while for the parabolic case the surfaces of constant $(a - t)$ must be used.

The above results hold everywhere except possibly at the origin. The calculation is now done specifically for the origin in the chosen parabolic model.

The surfaces of constant $(a - t)$ have a normal vector, n_α , which is calculated from

$$n_\alpha \propto \partial_\alpha (a - t) = (1, -a', 0, 0)$$

and the condition, $n_\alpha n^\alpha = \kappa$, where $\kappa = +1, 0$, or -1 , depending on whether the surface is timelike, null, or spacelike, respectively. It is found to be

$$n_\alpha = R' \sqrt{\frac{\kappa}{a'^2 - R'^2}} (1, -a', 0, 0), \quad (6.5)$$

where R' is given by eq (2.13), and it is understood that the term under the square root is set to unity if $\kappa = 0$. The tangent vector, u^α , found from $u^\alpha n_\alpha = 0$, and $u^\alpha u_\alpha = -\kappa$, is

$$u^\alpha = \sqrt{\frac{\kappa}{a'^2 - R'^2}} (a', 1, 0, 0). \quad (6.6)$$

The value of κ is determined by the sign of $(a'^2 - R'^2)$, but, since a' must be positive, the surface is always simultaneous or outgoing in the comoving frame, in the sense that as r increases along the surface the time never decreases.

The ratio R'/a' is given by eqs (2.13) and (3.3), as

$$\frac{R'}{a'} = \frac{g^2 r^{1-m}}{4ma_1} + \frac{2r}{g}, \quad (6.7)$$

and, if its absolute value is larger than 1, the surface is spacelike, while if it equal to or less than 1, the surface is null or timelike, respectively. Now it is necessary to approach the point $r = 0$, $g = 0$ along some definite path, since both terms of eq (6.7) are otherwise undefined at this point. Therefore, let the path be of the form

$$g = br^n, \quad n > 0, \quad (6.8)$$

where b is now a constant, so that (6.7) becomes

$$\frac{R'}{a'} = \frac{b^2}{4ma_1} r^{2n-m+1} + \frac{2}{b} r^{1-n}. \quad (6.9)$$

The types of behaviour of (6.9) may be conveniently divided up as follows.

(I). $R'/a' \rightarrow 0$, so that the surface is timelike. This is the case if $2n - m + 1 > 0$ and $1 - n > 0$, which leads to the conditions

$$m < 3, \quad n < 1, \quad n > \frac{m-1}{2}. \quad (6.10)$$

(II). $R'/a' \rightarrow \text{const}$, which may give all three results for ε . There are three separate conditions for this case.

(a) $2n - m + 1 = 0$ and $1 - n > 0$, which implies

$$m < 3, \quad n < 1, \quad n = \frac{m-1}{2}, \quad (6.11)$$

and the surface is spacelike, null, or timelike, depending on whether b is greater than, equal to, or less than $(4ma_1)^{1/2}$.

(b) $2n - m + 1 > 0$ and $1 - n = 0$, which gives

$$m < 3, \quad n = 1, \quad (6.12)$$

so that if b is less than, equal to, or greater than 2, then the surface is spacelike, null or timelike.

(c) $2n - m + 1 = 0$ and $1 - n = 0$, yielding

$$m = 3, \quad n = 1. \quad (6.13)$$

In this case the surface is spacelike if

$$b^3 - 12a_1b + 24a_1 = \Psi > 0,$$

Thus a spacelike surface is the only possibility if $a_1 < 9/4 = a_{1,B}$, but otherwise there is a range of b values between the two positive roots of Ψ (b_- and b_+) for which the surface is timelike, or null at the ends of that range. For $a_1 = a_{1,B}$ and $b_+ = b_- = b_B = 3$ the surface is null.

(III). $R'/a' \rightarrow \pm\infty$, so that the surface is spacelike. There are two possibilities here.

(a) $2n - m + 1 < 0$, in other words

$$\text{any } m, \quad n < \frac{m-1}{2}. \quad (6.14)$$

(b) $1 - n < 0$, implying

$$\text{any } m, \quad n > 1. \quad (6.15)$$

These results are summarised in a different order in table 1.

The orientations observed by travelling along the three asymptotic rays (one incoming and two outgoing) of (5.1) and (5.2) and along the central comoving world line are as follows:

(a)(i) $m < 3, n = m/3, \varepsilon = \pm 1$, satisfying (6.10), \Rightarrow the critical rays see a timelike crunch surface;

(a)(ii) $m < 3, n = 1, b = 2$, satisfying (6.12), \Rightarrow the post critical rays see an outgoing null crunch surface;

$m < 3, n = 0, b = 0$, satisfying (6.14), \Rightarrow the particle at $r = 0$ sees a spacelike crunch surface.

These clearly conflict with the representation of the ESC singularity in the causal diagram, fig 4, and are difficult to make sense of.

Table 1. Orientation of the crunch surface
for different paths of approach to the origin.

$m < 3$	$n < 1$	$n < \frac{m-1}{2}$		spacelike
		$n = \frac{m-1}{2}$	$b^2 > 4ma_1$	spacelike
			$b^2 = 4ma_1$	null
			$b^2 < 4ma_1$	timelike
		$n > \frac{m-1}{2}$		timelike
	$n = 1$		$b > 2$	timelike
			$b = 2$	null
			$b < 2$	spacelike
	$n > 1$			spacelike
$m = 3$	$n < 1$			spacelike
	$n = 1$	$a_1 < a_{1,B}$		spacelike
		$a_1 = a_{1,B}$	$b \neq b_B$	spacelike
			$b = b_B$	null
		$a_1 > a_{1,B}$	$b > b_+$	spacelike
			$b = b_+$	null
			$b_- < b < b_+$	timelike
			$b = b_-$	null
			$b < b_-$	spacelike
	$n > 1$			spacelike
$m > 3$				spacelike

7 Continuity at the Origin

A possible physical reason for the appearance of the ESC singularity remains elusive. It may be that the problem is merely one of insufficient continuity through the origin, but this needs to be demonstrated at events earlier than the big crunch. The origin of the value $m = 3$, is clearly the choice made in eq (2.9) for the form of the function $F(r)$, so one obvious physical property that changes on either side of $m = 3$, is the rate of accumulation of mass onto the crunch surface, which is easily derived from the two arbitrary functions, a and F , as $dM/dt = F'/2a' = 3r^{3-m}/2ma_1$. Thus for $m < 3$, the initial rate of accumulation of mass onto the singularity is zero, for $m > 3$ it is divergent, and for $m = 3$ it is finite. The borderline values, $a_{1,A}$, and $a_{1,B}$, yield no special values of dM/dt , however.

A continuity condition is now suggested which excludes all models that will develop an ESC singularity (as well as all self similar models). The condition is that, on some constant time slice, $t = \text{const}$, the density, ρ , expressed as a function of the mass, M , should be C^1 through the origin.

In other words, as $r \rightarrow 0$,

$$\left. \frac{\partial \rho}{\partial M} \right|_t \rightarrow 0, \quad (7.1)$$

and for the model of eqs (2.9) and (3.3), this becomes

$$\left. \frac{\partial \rho}{\partial M} \right|_t = 2 \left. \frac{\partial \rho}{\partial F} \right|_t \rightarrow \frac{128ma_1(4 - 2m + m^2)}{\pi g^9 r^{3-m}}. \quad (7.2)$$

Satisfying this continuity condition obviously requires

$$m > 3, \quad (7.3)$$

and eliminates all models containing an ESC singularity. This condition is expressed in terms of invariant physical quantities, and so is not coordinate dependent. More importantly, it applies at times prior to the crunch, including, for example, the initial conditions.

Although Christodoulou chose his r coordinate to be proportional to the proper radius near the origin, so that his continuity condition is invariant, it is apparent that the condition is not strong enough. At the origin, only the leading term in a Taylor expansion of the density is relevant to the formation of an ESC singularity, so it does not matter whether $\rho(r)$ is C^1 or C^∞ .

8 Discussion

It is evident then, that the crunch surface is completely spacelike for $m > 3$, and also for $m = 3$ and $a_1 < a_{1,B}$. But for the other cases, there is not a definite answer. What this multiplicity of results means is not clear, though it does seem to imply more structure than was revealed by the causal diagram. This would imply that such diagrams are not sufficient for displaying the full behaviour of the ESC singularity. The most puzzling point is that the causal diagram shows there is an incoming null section to the ESC singularity, from which all the post critical rays emerge, while the calculations of section 5 indicate that the crunch surface can only be simultaneous or outgoing. These results could possibly be reconciled if the comoving frame becomes incoming null at the critical point.

The causal diagrams that were calculated have an important difference from those of Eardley and Smarr in the existence of a jump in the u and v values across the incoming critical ray, but their conditions for the presence of an ESC singularity have been borne out, and extended to the case of non integer m . Another difference is that they find the crunch surface is totally spacelike for all models that are free of an ESC singularity, whereas it was shown above that the orientation of the crunch surface becomes ill defined with $m = 3$ and values of a_1 for which there are no critical or post critical rays present (though g' does become positive for outgoing rays in these cases).

The causal diagrams that have been derived for the ‘‘light focussing’’ singularity in some Vaidya spacetimes are very much like those of Eardley and Smarr for the ESC singularity in the Toman metric. However, there is a very real difference between the two in that the origin $r = 0$ is always singular in the Vaidya metric, so there is no possibility of rays passing through it.

There is still plenty of work to be done before this singularity is understood. It would be useful to calculate a causal diagram for some other cases, including a model without an ESC singularity, to show what features are always present, but particularly the $m = 3$ case with $a_{1,B} < a_1 < a_{1,A}$, mentioned above. It would also be of interest to calculate the behaviour of timelike and spacelike geodesics near ESC singularities, and it should be possible to use the approximate methods presented here. Newman (1985) has shown that there cannot be any rays emerging from the crunch surface at

points other than $r = 0$, but it would be interesting to know if there is distortion of the light paths near the crunch if $a'(r \neq 0) = 0$.

Finally, (7.1) is a new continuity condition, whose usefulness may well extend beyond the Tolman model. It is important to investigate other models that violate it, for behaviour similar to the ESC singularity.

References

- Bondi, H., 1947, *Mon. Not. Roy. Astron. Soc.* **107**, 410.
- Christodoulou, D. 1984, *Comm. Math. Phys.* **93**, 171.
- Datt, B. 1938, *Zeit. Phys.* **108**, 314.
- Eardley, D.M. 1974, *Phys. Rev. Lett.* **33**, 442.
- Eardley, D.M. and Smarr, L. 1979, *Phys. Rev. D* **19**, 2239.
- Hellaby, C. 1985, Ph.D. Thesis, Queen's University, Kingston, Ontario, Canada.
- Hellaby, C. and Lake, K. 1985, *Astrophys. J.* **290**, 381; and corrections in *ibid* **300**, 461.
- Hiscock, W.A., Williams, W.G., and Eardley, D.M. 1982, *Phys. Rev. D* **26**, 751.
- Kamke, E. 1944, "*Differential Gleichungen: Lösungsmethoden und Lösungen*", 3rd edition (Chelsea).
- Kuroda, Y. 1984, *Prog. Theor. Phys.* **72**, 63.
- Lake, K. 1988, *Phys. Rev. Lett.* **60**, 241.
- Lematre, G., 1933, *Ann. Soc. Scient. Bruxelles* **A53**, 51.
- Ori, A. and Piran, T. 1987, *Phys. Rev. Lett.* **59**, 2137.
- Waugh, B. and Lake, K. 1986, *Phys. Rev. D* **34**, 2978.
- Waugh, B. and Lake, K. 1988, *Phys. Rev. D* **38**, to appear.
- Newman, R.P.A.C. 1986, *Class. Quantum Grav.* **3**, 527.
- Papapetrou, A. 1985, "*Formation of a Singularity and Causality*", in "*A Random Walk in Cosmology*", Eds. Dadhich, Rao, Narlikar, and Vishveshwara, Wiley Eastern.
- Tolman, 1934, *Proc. Nat. Acad. Sci.* **20**, 169.

Figures

Fig 1. The paths of the radial light rays near the ESC singularity are shown in the s - q plane. The three diagrams are the same thing on three different scales. Though negative s (radius) values are not strictly possible, this diagram plots incoming rays on the left of $s = 0$, and outgoing rays on the right. Since light rays do pass through $s = 0$, this gives a realistic picture of a slice through the origin, except that the right to left rays have been suppressed.

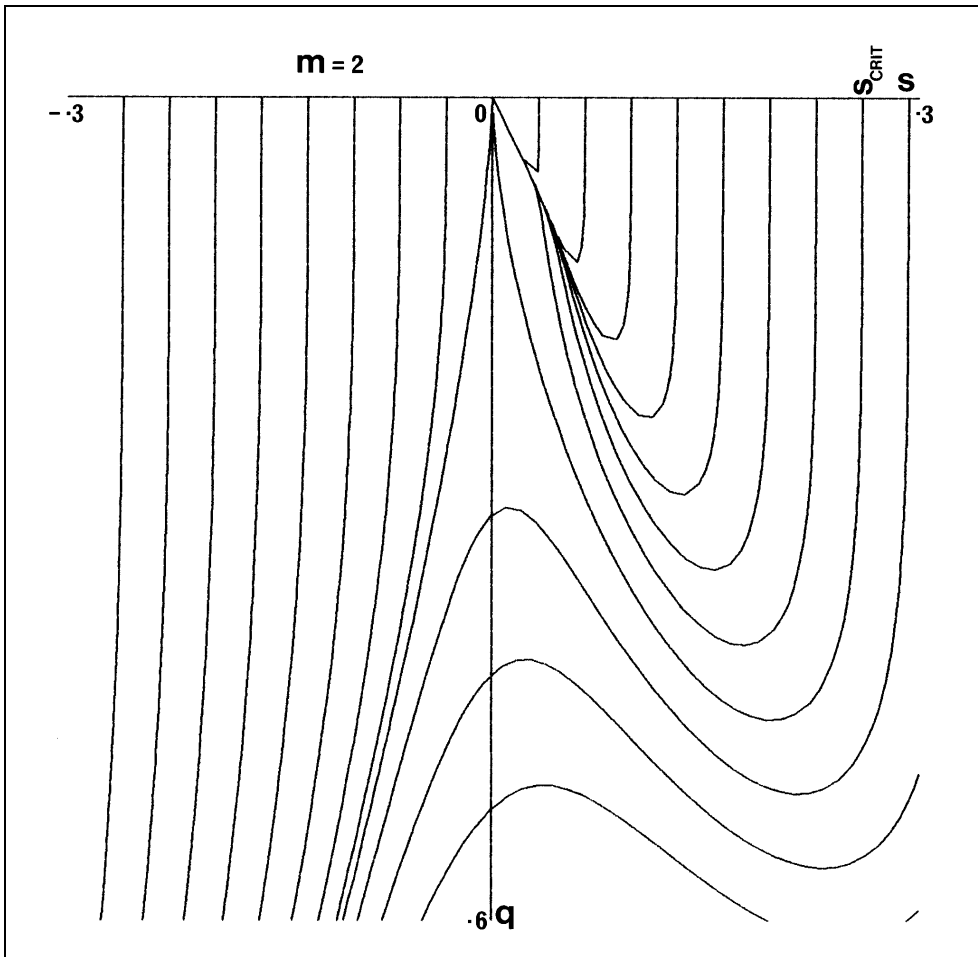


Fig. 1(a)

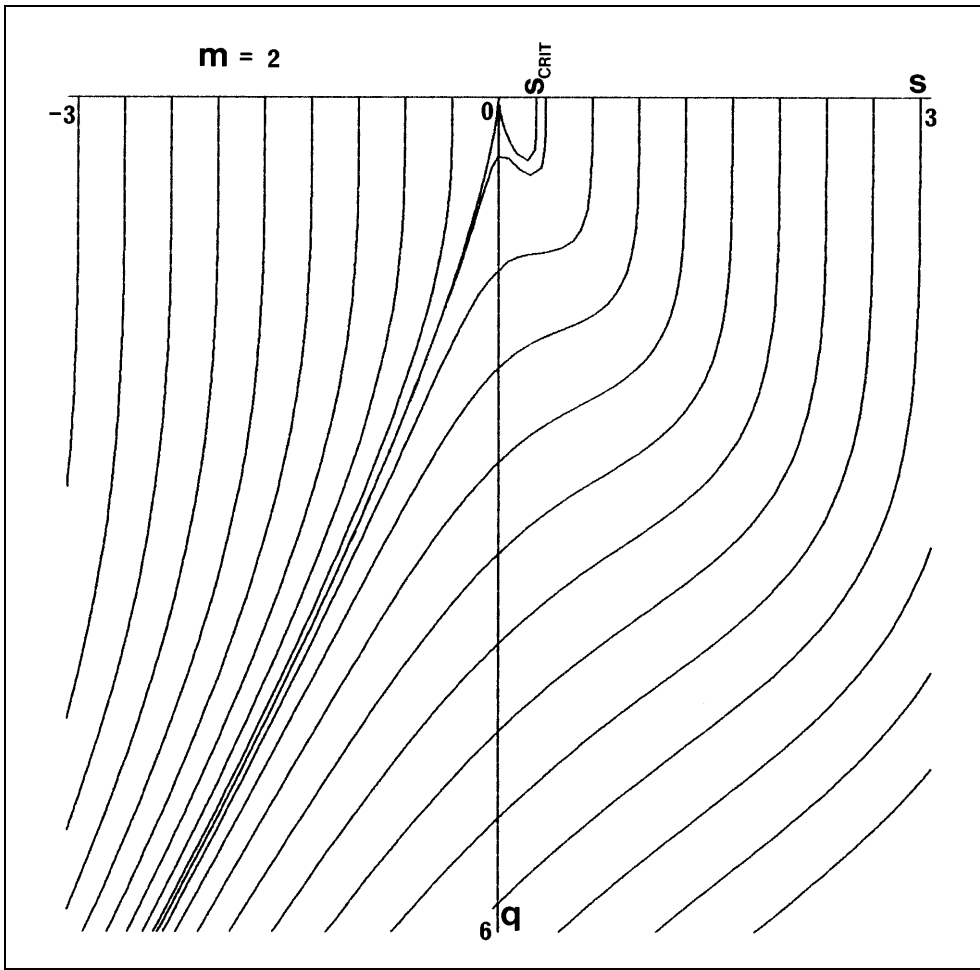


Fig. 1(b)

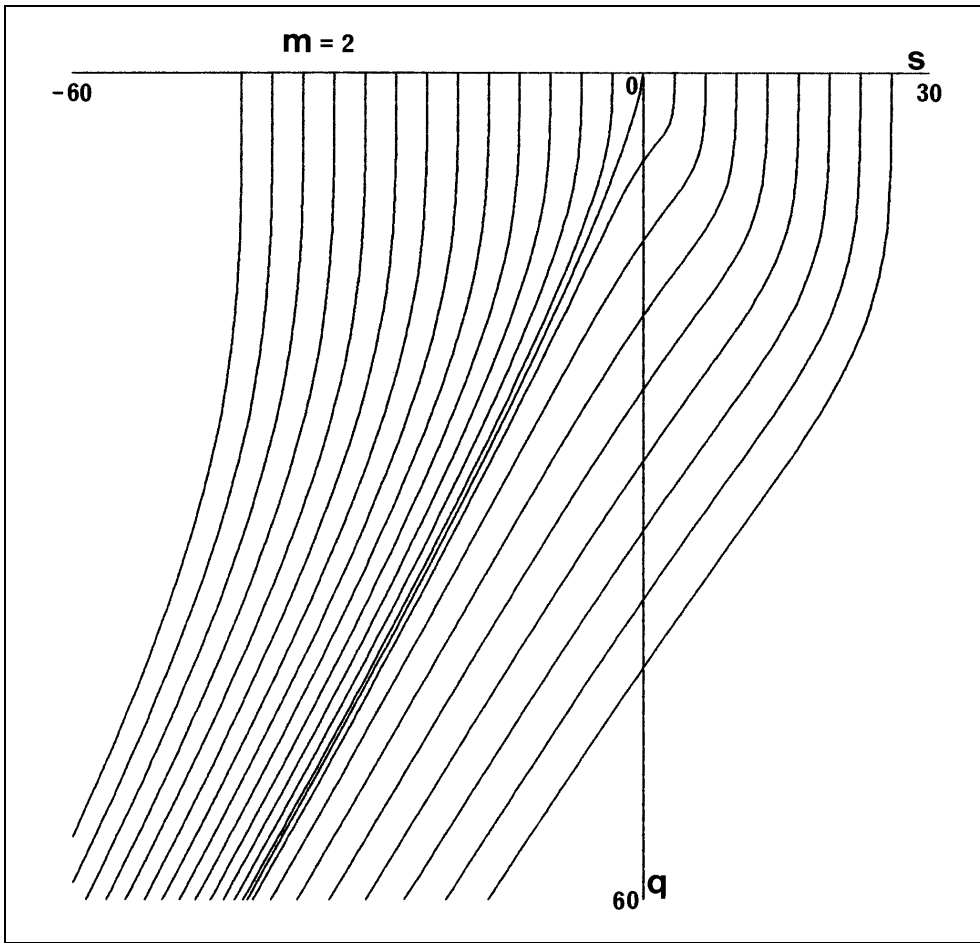


Fig. 1(c)

Fig 2. The paths of the radial light rays near the ESC singularity in the $r-t$ plane. The same curves as in fig 1 are shown for three comparable scales.

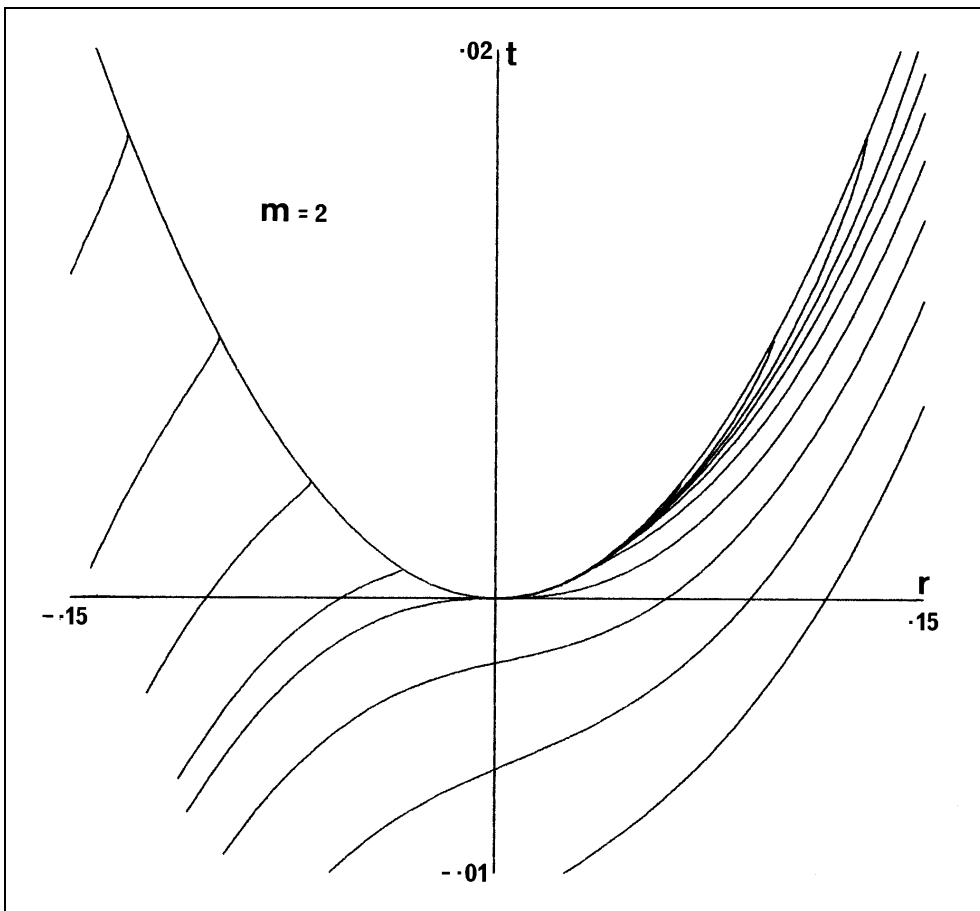


Fig. 2(a)

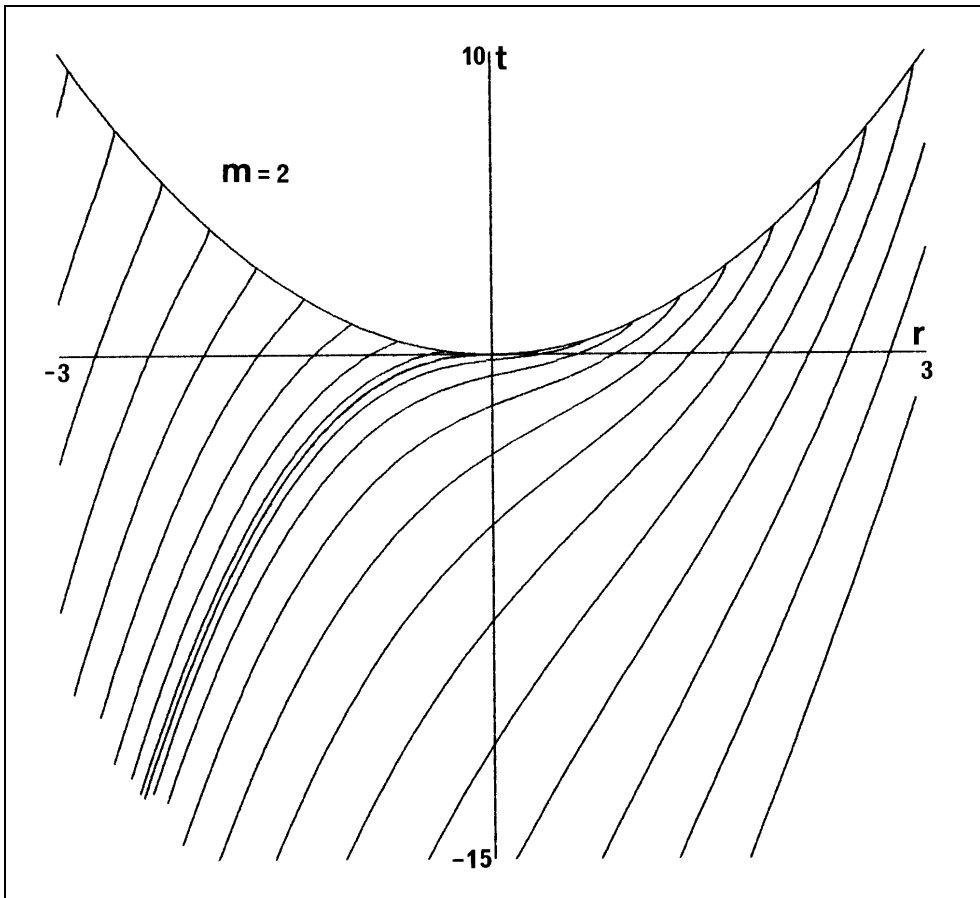


Fig. 2(b)

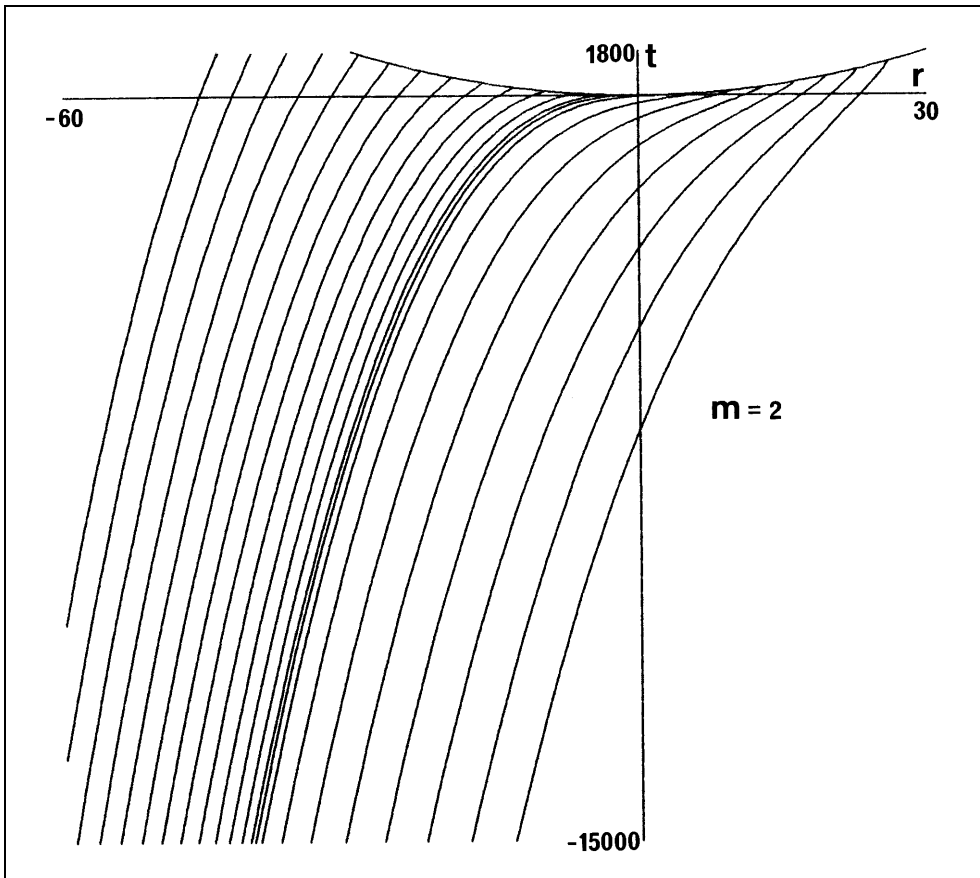


Fig. 2(c)

Fig 3. Sketch of the s grid and ray integration procedure, showing recorded data points.

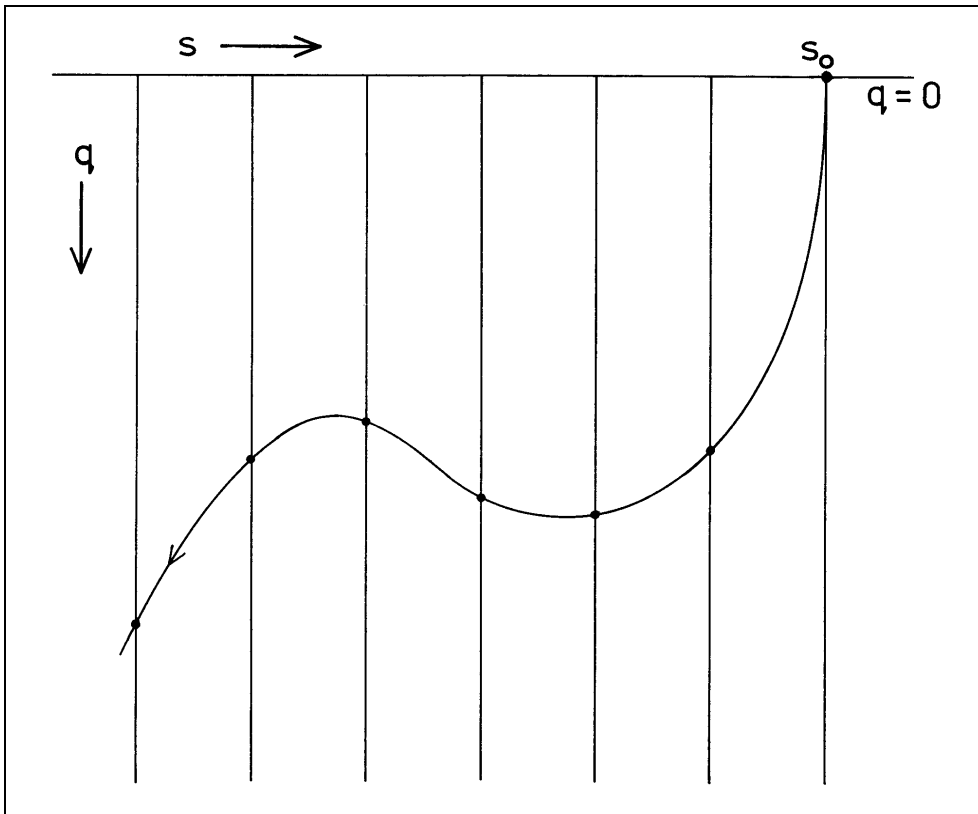


Fig 4. The causal diagram for a parabolic Tolman model with arbitrary functions given by eqs (2.9) and (3.3) with $m = 2$, showing the region near the ESC singularity. Diagrams (a) to (e) show the curves of constant s , q , t , R , and ρ , respectively in the u - v plane. The light rays follow lines of constant u or constant v , and the origin is the central vertical line.

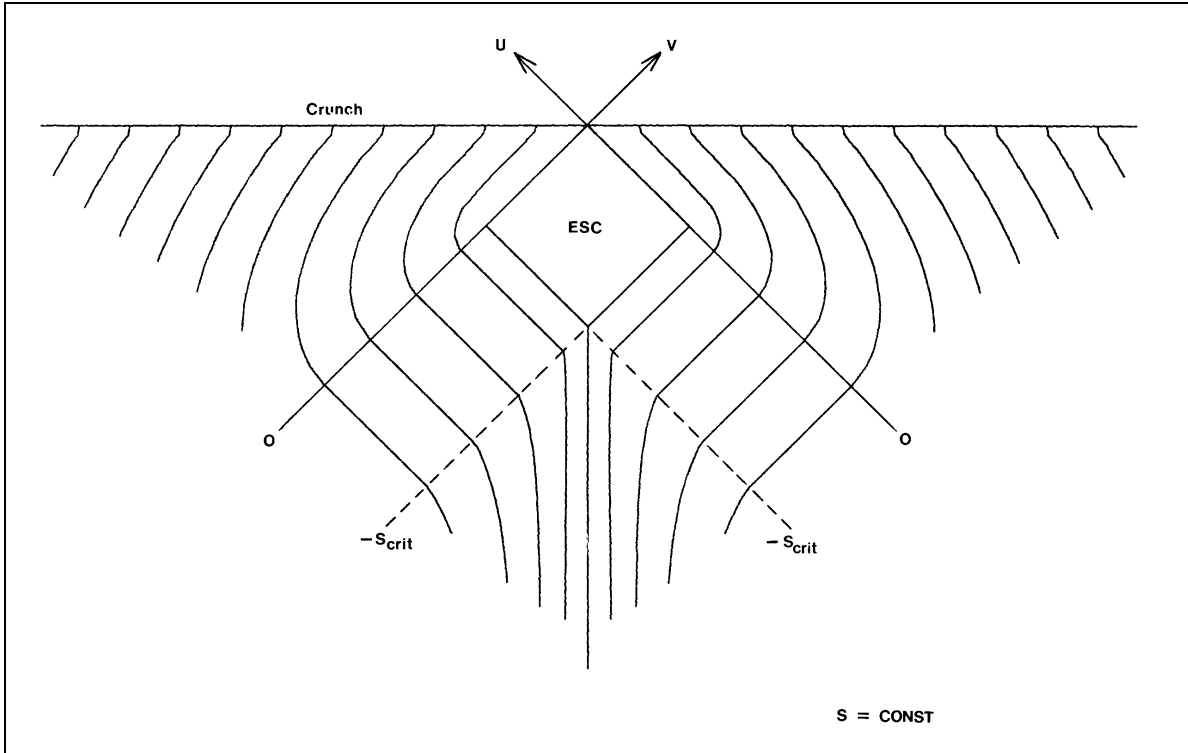


Fig. 4(a)

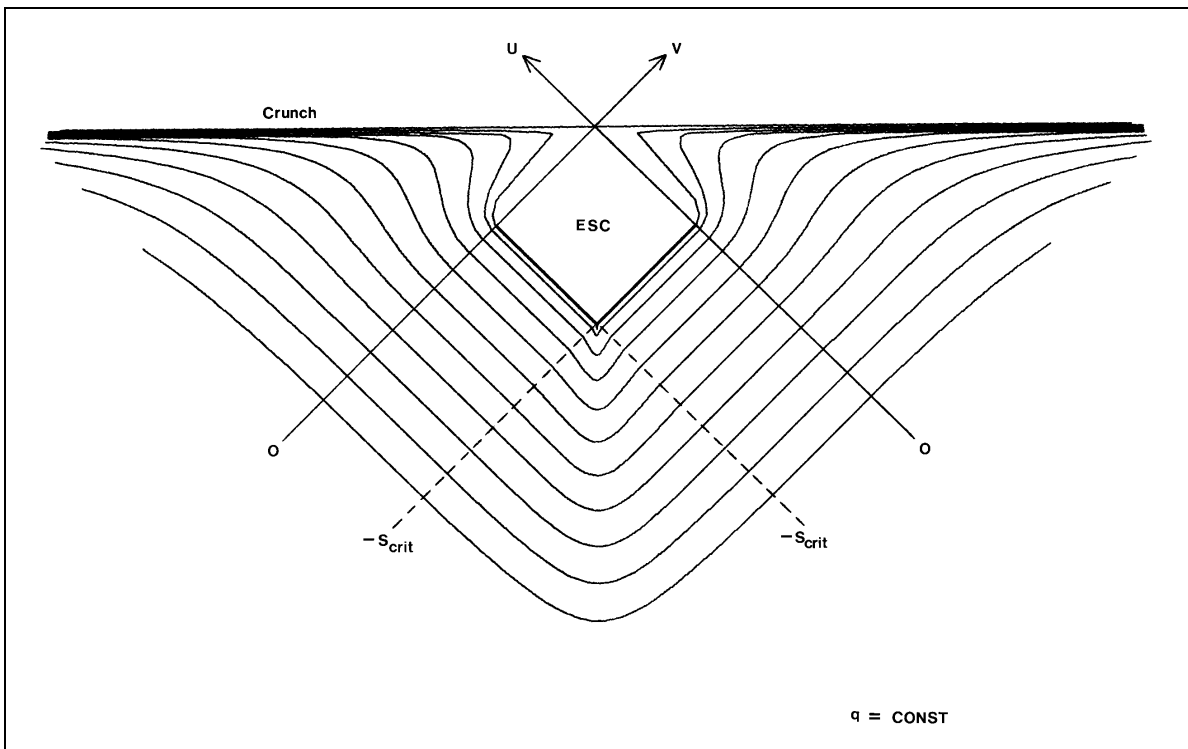


Fig. 4(b)

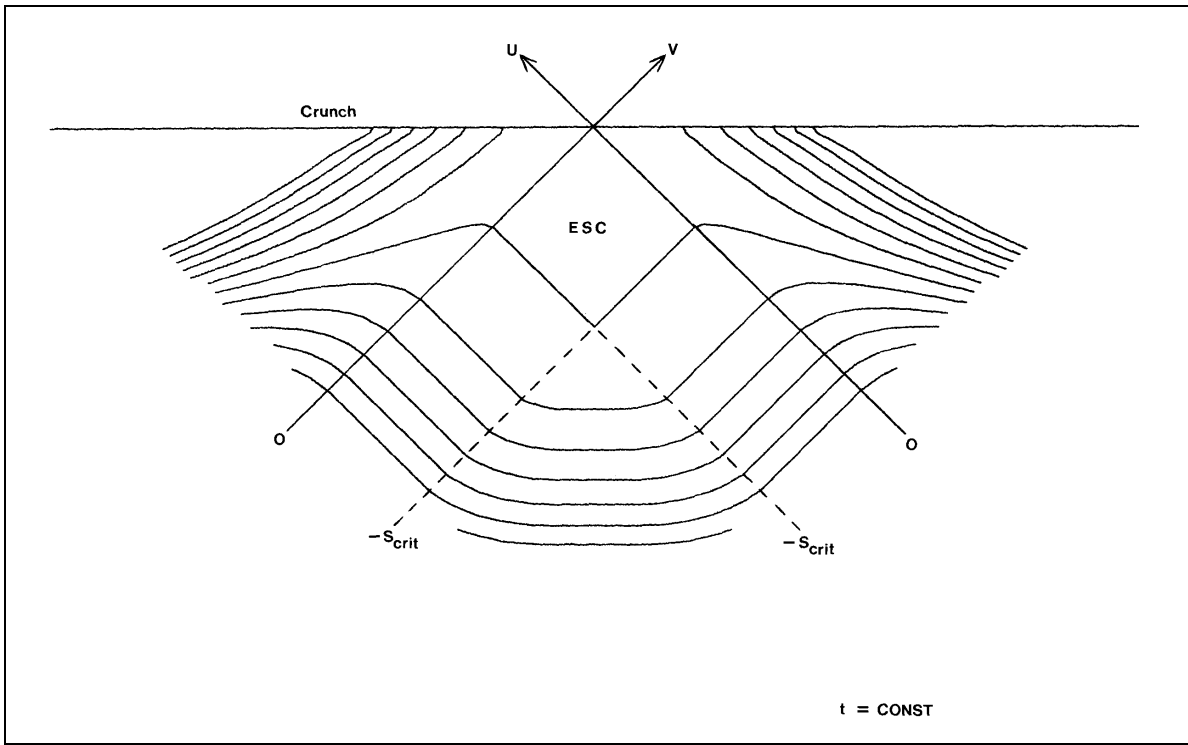


Fig. 4(c)

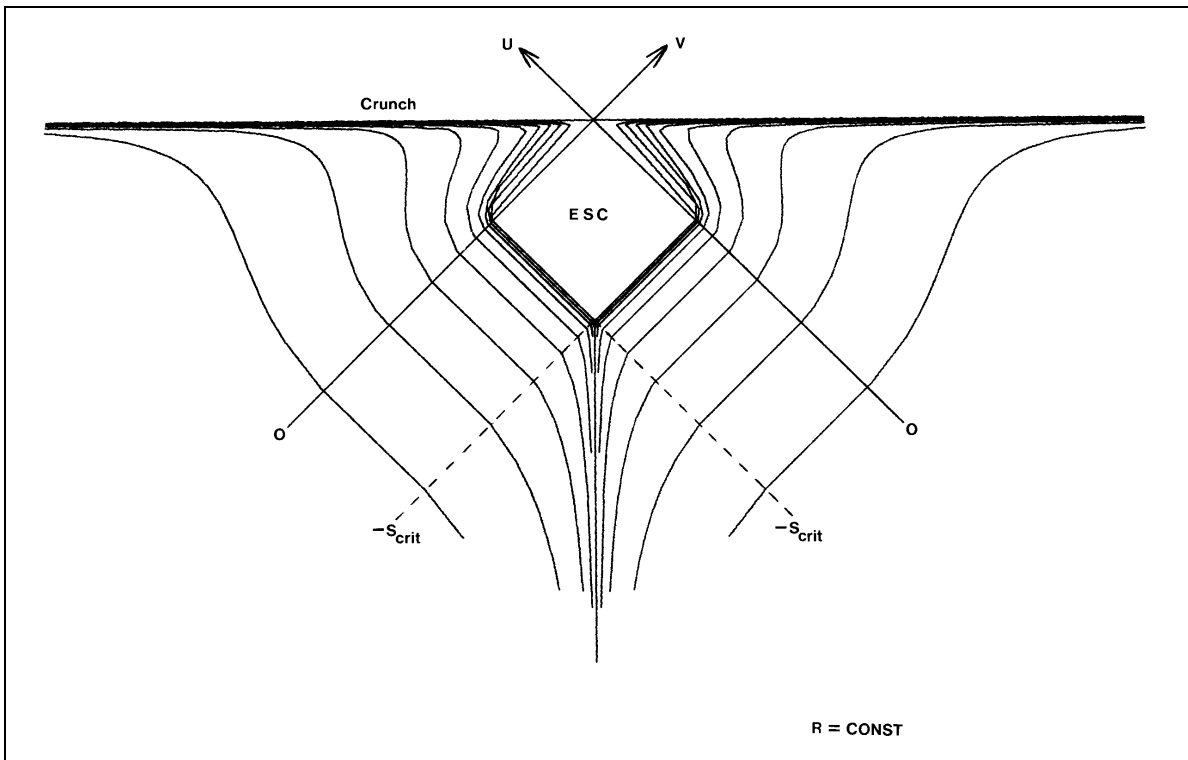


Fig. 4(d)

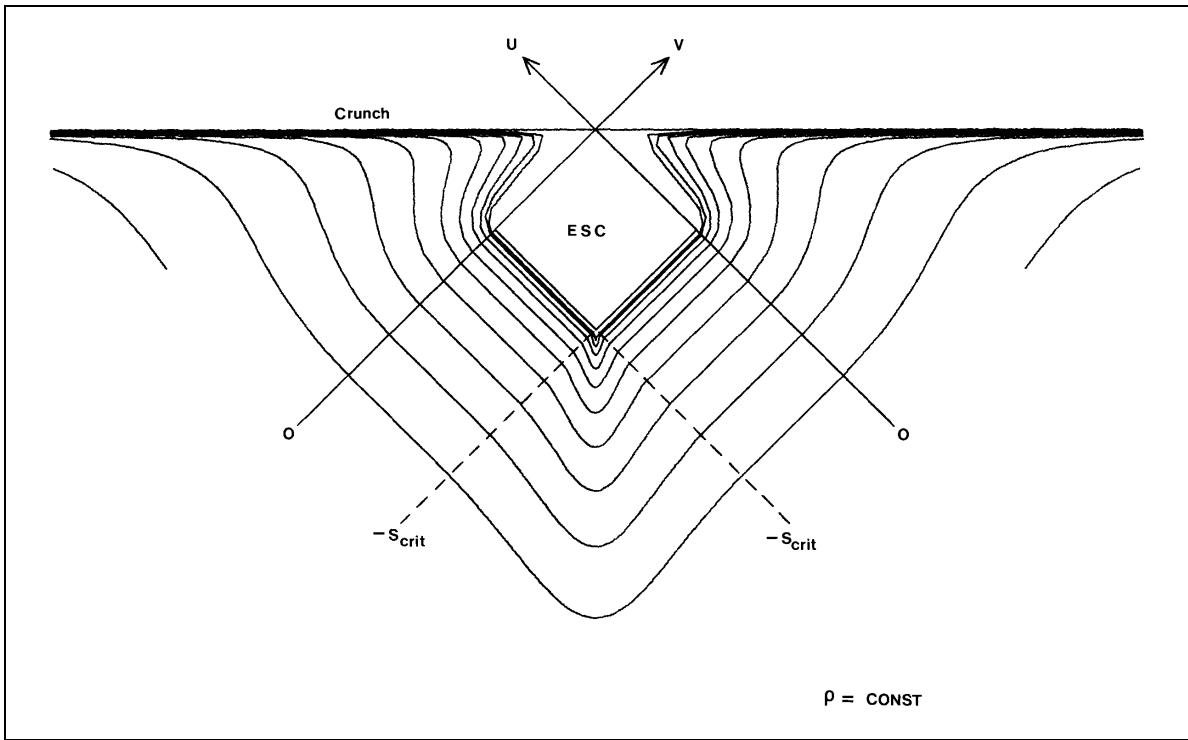


Fig. 4(e)

Fig 5. The paths of the radial light rays near the ESC singularity are shown in the s - q plane, for $m = 1, 1.5,$ and 2.5 . All three have been scaled so that s_{crit} is the same size in each diagram.

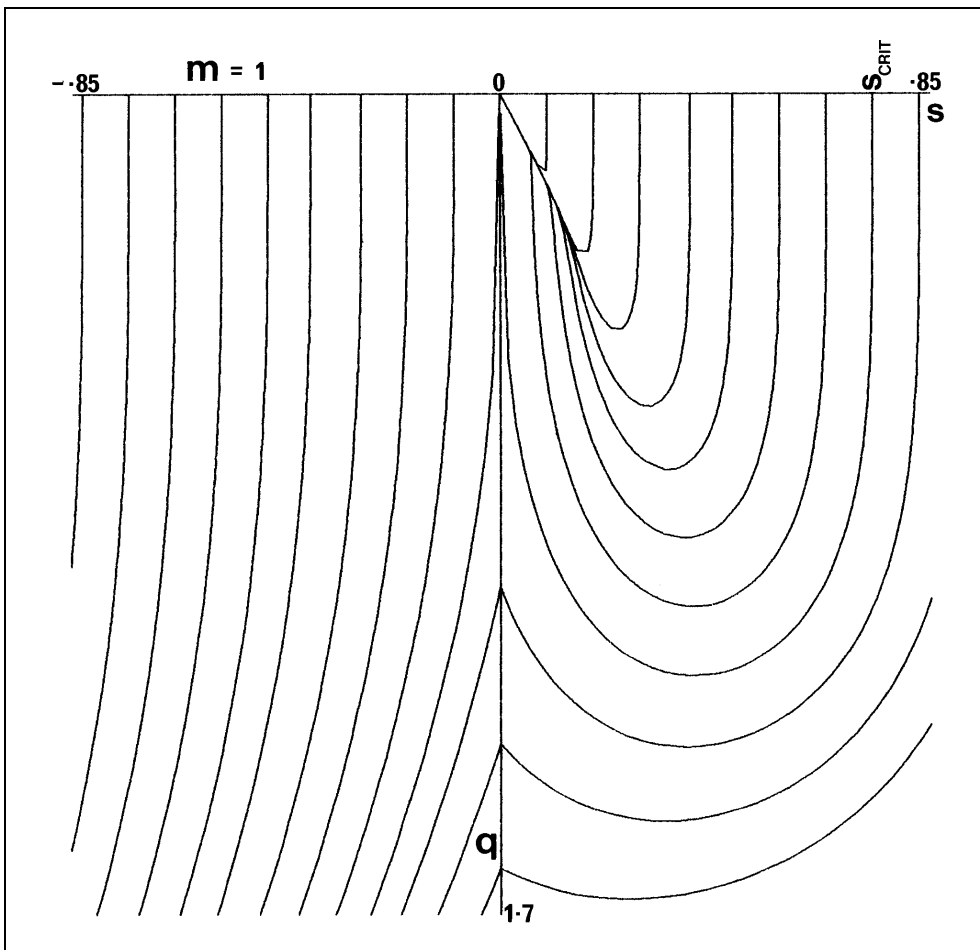


Fig. 5(a)

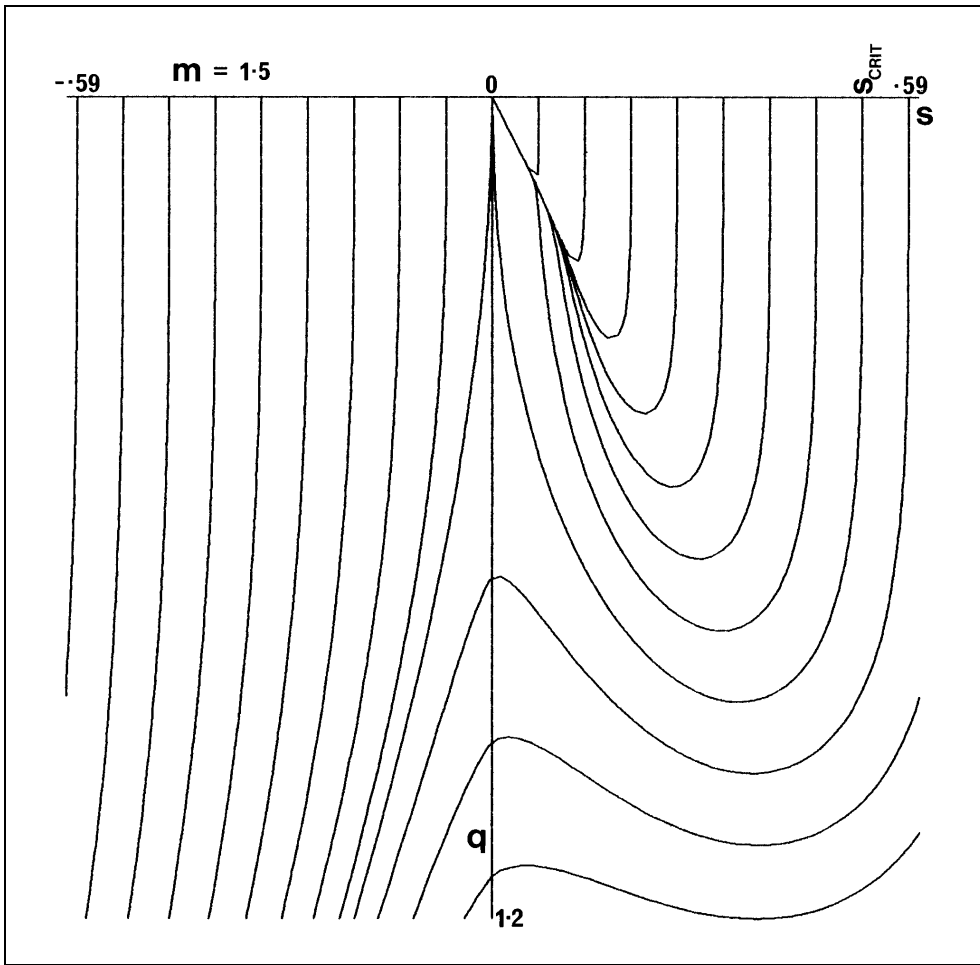


Fig. 5(b)

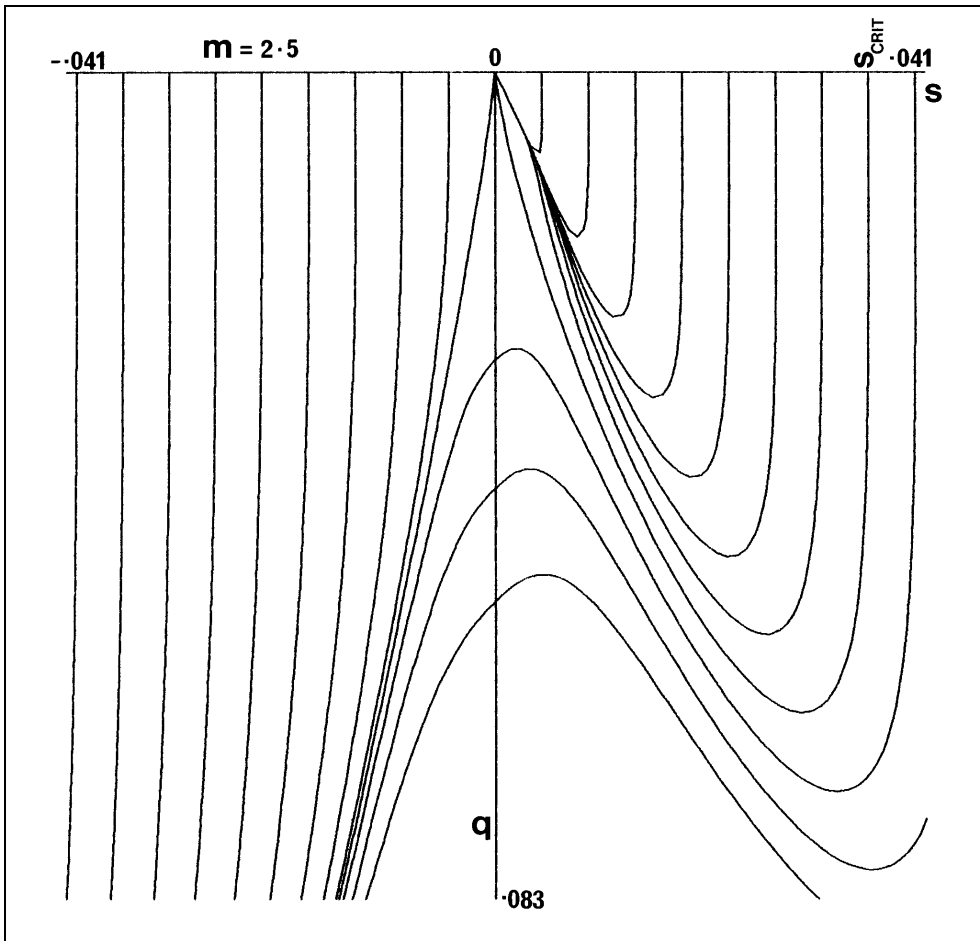


Fig. 5(c)

Fig 6. The paths of the radial light rays near the ESC singularity are shown in the $r-t$ plane, for $m = 1, 1.5,$ and 2.5 . The curves are the same as in fig 5.

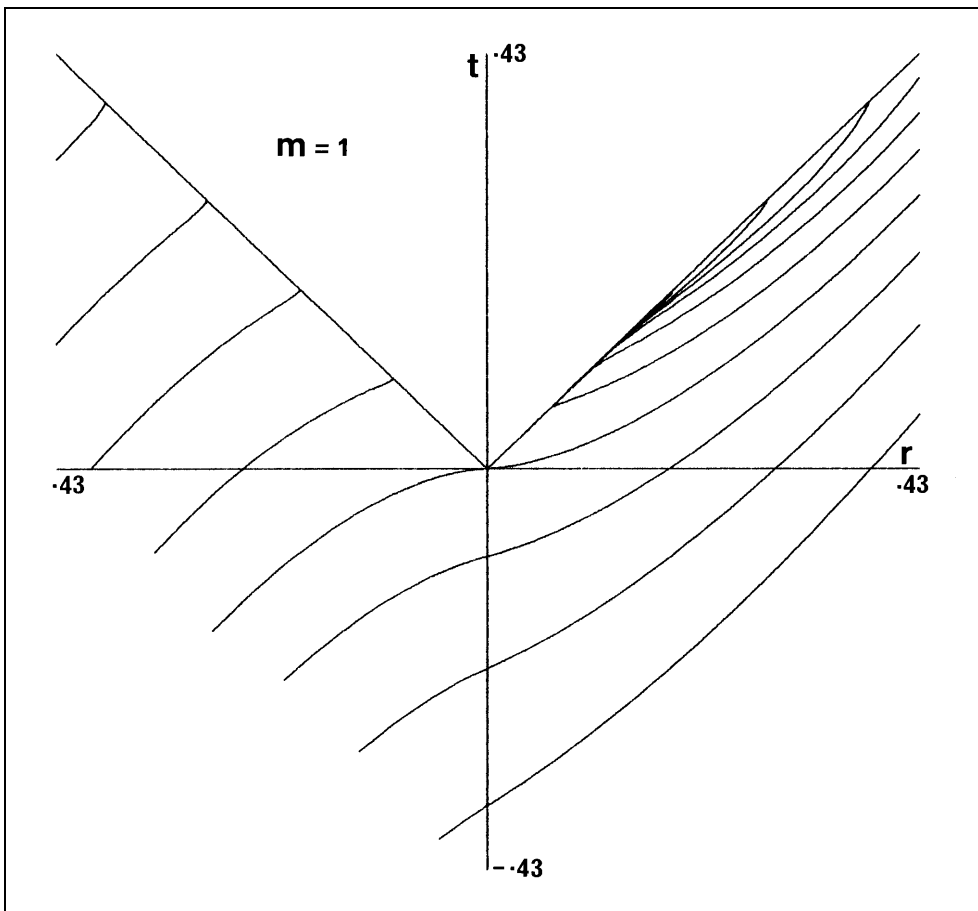


Fig. 6(a)

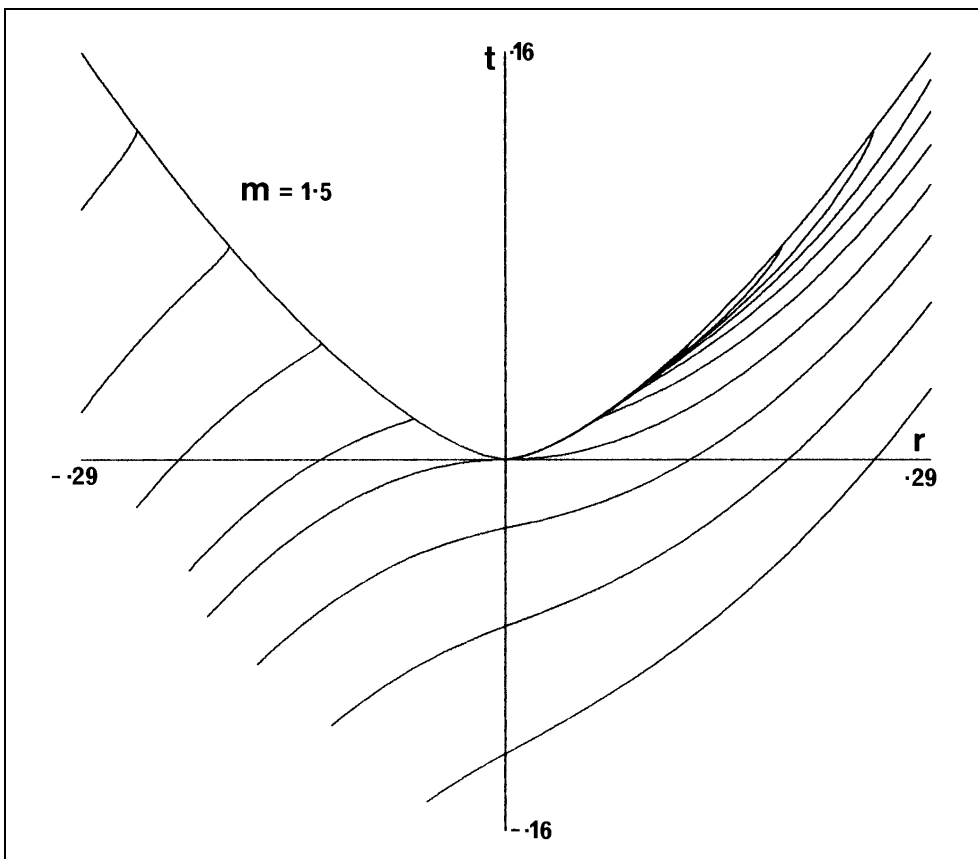


Fig. 6(b)

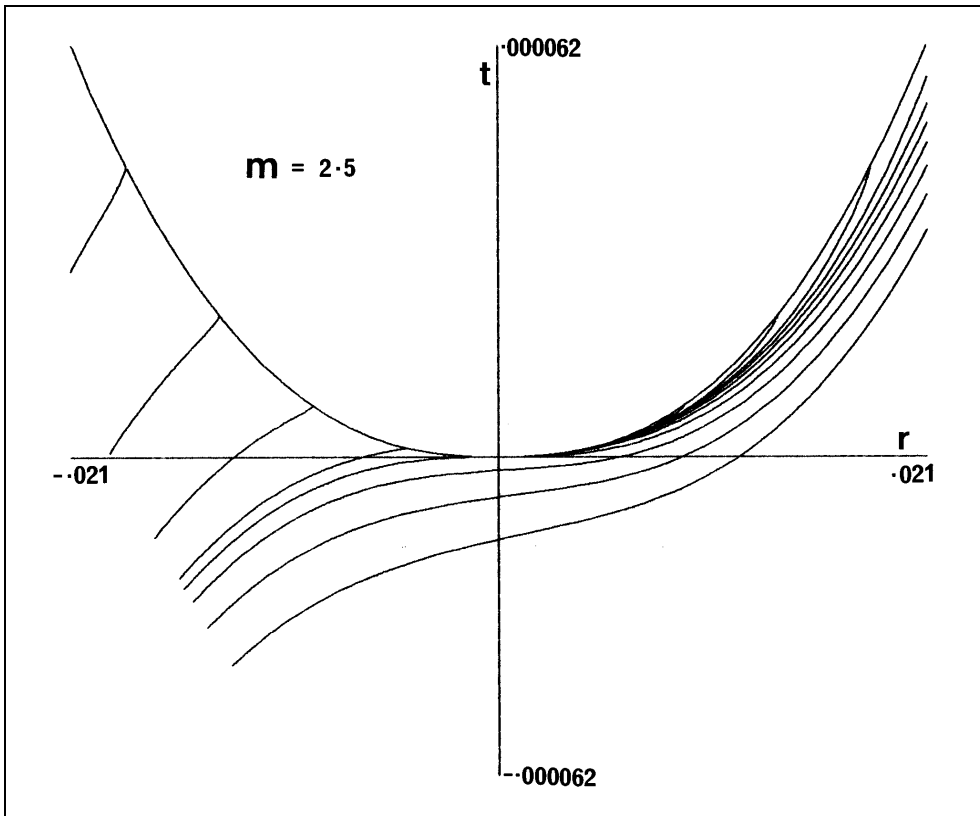


Fig. 6(c)

Fig 7. The outgoing critical rays in the s - q plane for several values of m between 1 and 2.6, shown on the same scale.

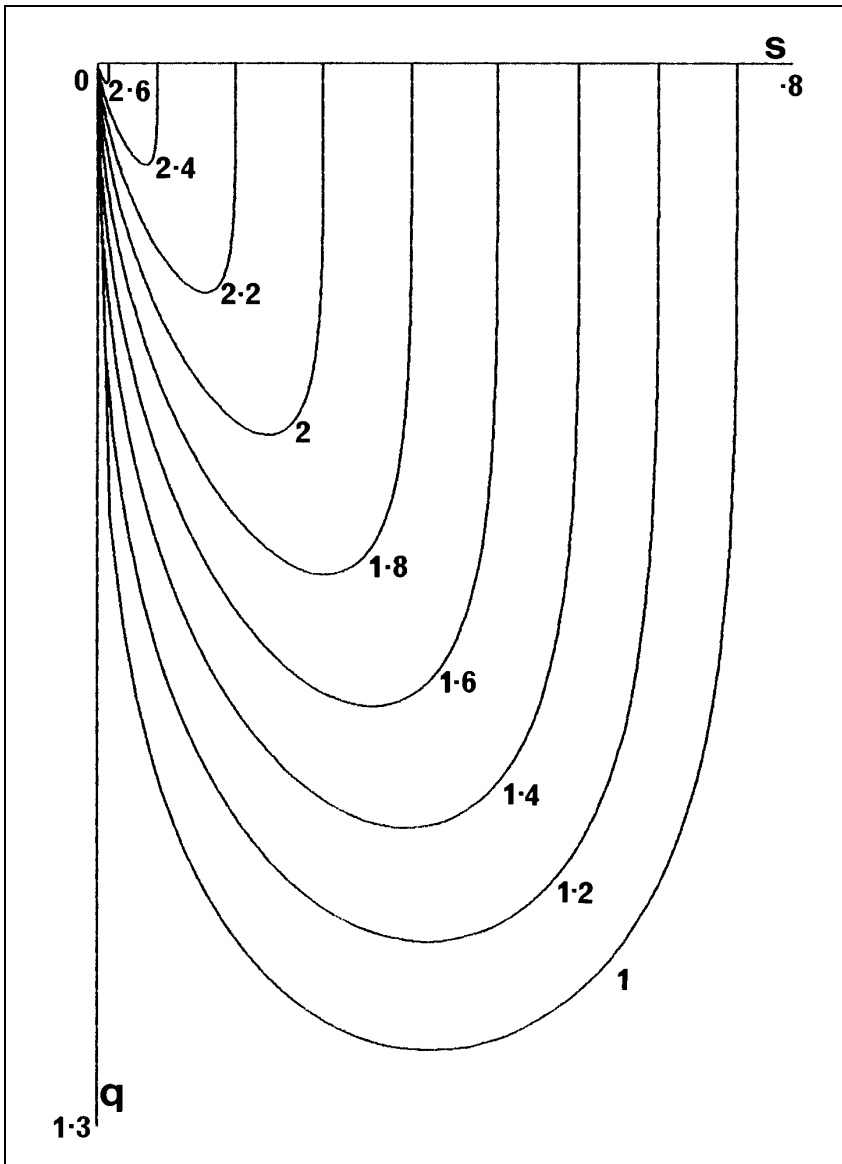


Fig 8. The critical radius, s_{crit} , as a function of m , in the range 1 to 2.6.

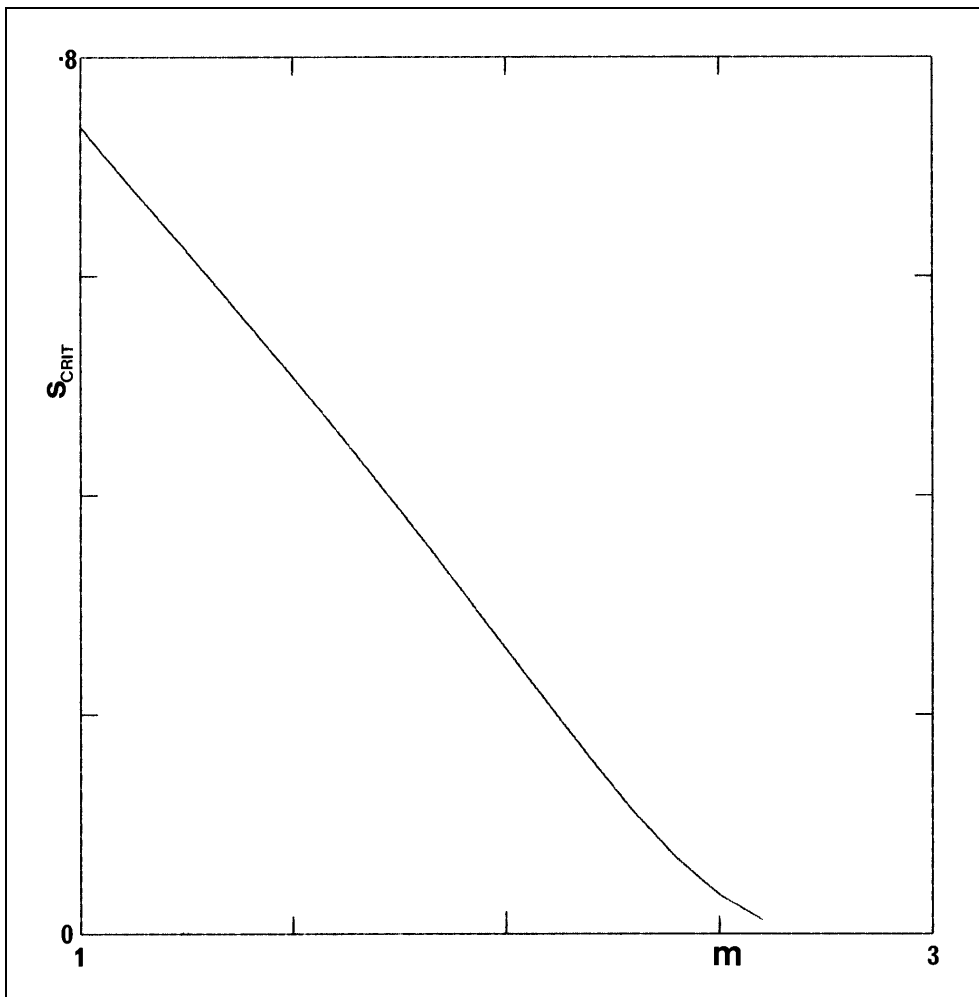


Fig 9. The ratio M_{crit}/t_{crit} as a function of m .

